International Journal of Pharmaceutics 407 (2011) 111–118

Contents lists available at ScienceDirect

International Journal of Pharmaceutics

journal homepage: www.elsevier.com/locate/ijpharm

Differences in crystallization rate of nitrendipine enantiomers in amorphous solid dispersions with HPMC and HPMCP

Tamaki Miyazaki[a,*], Yukio Aso[a], Sumie Yoshioka[b], Toru Kawanishi[a]

[a] Division of Drugs, National Institute of Health Sciences, 1-18-1 Kamiyoga, Setagaya-ku, Tokyo 158-8501, Japan
[b] School of Pharmacy, University of Connecticut, Storrs, CT, United States

ARTICLE INFO

Article history:
Received 21 October 2010
Received in revised form
21 December 2010
Accepted 19 January 2011
Available online 26 January 2011

Keywords:
Nitrendipine
Enantiomer
Chiral polymer
Solid dispersions
Crystallization

ABSTRACT

To clarify the contribution of drug–polymer interaction to the physical stability of amorphous solid dispersions, we studied the crystallization rates of nitrendipine (NTR) enantiomers with identical physicochemical properties in the presence of hydroxypropylmethylcellulose (HPMC), hydroxypropylmethylcellulose phthalate (HPMCP) and polyvinylpyrrolidone (PVP). The overall crystallization rate at 60 °C and the nucleation rate at 50–70 °C of (+)-NTR were lower than those of (−)-NTR in the presence of 10–20% HPMC or HPMCP. In contrast, similar crystallization profiles were observed for the NTR enantiomers in solid dispersions containing PVP. The similar glass transition temperatures for solid dispersions of (−)-NTR and (+)-NTR suggested that the molecular mobility of the amorphous matrix did not differ between the enantiomers. These results indicate that the interaction between the NTR enantiomers and HPMC or HPMCP is stereoselective, and that differences in the stereoselective interaction create differences in physical stability between (−)-NTR and (+)-NTR at 50–70 °C. However, no difference in physical stability between the enantiomers was obvious at 40 °C. Loss of the difference in physical stability between the NTR enantiomers suggests that the stereoselective interaction between NTR and the polymers may not contribute significantly to the physical stabilization of amorphous NTR at 40 °C.

1. Introduction

Nifedipine analogues are used for treatment of cardiovascular disorders. Most of them are poorly water soluble and their bioavailability is low when administered orally in crystal form. To improve the bioavailability by increasing the dissolution rate and solubility, amorphous solid dispersions of nifedipine analogues have been studied over the past few decades (Suzuki and Sunada, 1998; Chutimaworapan et al., 2000; Vippagunta et al., 2002; Hirasawa et al., 2003a,b, 2004; Tanno et al., 2004; Karavas et al., 2005, 2006; Wang et al., 2005, 2007; Kim et al., 2006; Konno and Taylor, 2006; Huang et al., 2008; Marsac et al., 2008; Rumondor et al., 2009a,b). Drugs in an amorphous state are more easily dissolved in water than their crystalline counterparts. However, recrystallization to a thermodynamically stable form during long-term storage is a matter of concern. The physical stability of amorphous solid dispersions (crystallization tendency) has been reported to correlate with several factors, such as molecular mobility (Aso et al., 2004; Miyazaki et al., 2007), drug–excipient interactions and miscibility (Matsumoto and Zografi, 1999; Marsac et al., 2006, 2009; Miyazaki et al., 2004, 2006, 2007; Konno and Taylor, 2006; Haddadin et al., 2009; Tao et al., 2009; Telang et al., 2009). The crystallization rate of amorphous nitrendipine (NTR) increases with a decrease in the glass transition temperature (T_g) associated with water sorption, indicating that molecular mobility, in terms of T_g, is correlated with physical stability. However, amorphous nilvadipine is more stable than nifedipine, even though the two had similar T_g values, indicating that the difference in physical stability between nilvadipine and nifedipine might be attributable to differences in chemical structure (Miyazaki et al., 2007). Hydrogen bond interaction between felodipine and hydroxypropylmethylcellulose (HPMC) or hydroxypropylmethylcellulose acetate succinate is considered to decrease the nucleation rate of felodipine, since no significant change in molecular mobility, reflected in T_g value, has been observed (Konno and Taylor, 2006). Also, drug–excipient miscibility is reportedly related to the physical stability of nifedipines. Drug crystallization has been observed to occur earlier in solid dispersions showing phase separation due to low miscibility of the drug with the excipient polymers (Rumondor et al., 2009a,b; Marsac et al., 2010). In order to develop stable amorphous solid dispersions, it is important to clarify the relative significance of these factors for the physical stability of amorphous solid dispersions. Therefore, designing a model system that is as simple as possible is the key to evaluation of each individual factor.

NTR has an asymmetric carbon (Fig. 1), and is available as a mixture of both enantiomers. These enantiomers can be resolved by chiral chromatography. Since both enantiomers have identical physical and chemical properties, including molecular mass, T_g,

* Corresponding author. Tel.: +81 3 3700 1141; fax: +81 3 3707 6950.
E-mail address: miyazaki@nihs.go.jp (T. Miyazaki).

0378-5173/$ – see front matter © 2011 Elsevier B.V. All rights reserved.
doi:10.1016/j.ijpharm.2011.01.035

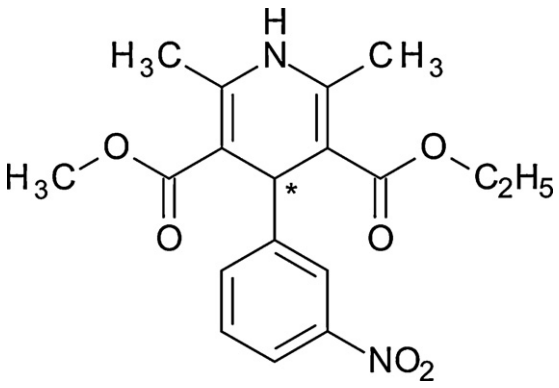

Fig. 1. Chemical structure of NTR. The asterisk represents asymmetric carbon.

melting point and density, the effects of molecular mobility and chemical structure on their physical stability are expected to be the same. Therefore, solid dispersions of NTR enantiomers may provide a useful model system for studies of drug–polymer stereoselective interaction. In the present study, HPMC and hydroxypropylmethylcellulose phthalate (HPMCP) were used as chiral polymers, and polyvinylpyrrolidone (PVP), an achiral polymer, was selected as a control to investigate the effect of drug–polymer interaction on the physical stability of amorphous NTR enantiomers. The overall crystallization rates were determined from the time-profiles of amorphous drug remaining, as measured by differential scanning calorimetry (DSC). Furthermore, the nucleation and the crystal growth rates of each NTR enantiomer in the solid dispersions containing HPMC, HPMCP or PVP were determined by polarized light microscopy. Measurements of T_g and Fourier-transform infrared spectra (FT-IR) were carried out for evaluation of molecular mobility and drug–polymer interactions, respectively.

2. Materials and methods

2.1. Materials

PVP (PVP10) and HPMC (USP grade) were purchased from Sigma–Aldrich, Inc. HPMCP (HP-55) was kindly obtained from Shin-Etsu Chemical Co., Ltd.

NTR (Wako Pure Chemical Industries Ltd.) was resolved on a CHIRALCEL OJ-H column (Daicel Chemical Industries, Ltd., 10 mm × 250 mm) into two fractions of each enantiomer with a mobile phase of n-hexane/ethanol (100/15, flow rate: 4 ml/min). A 500 μl of 1% NTR solution in n-hexane/ethanol (1/1) was injected, and ultraviolet spectrophotometric detection was carried out at 254 nm. The circular dichroism spectrum of the first fraction exhibited a negative peak at around 360 nm, and the second one exhibited a positive peak. Therefore, the first and second fractions of NTR were designated (−)-NTR and (+)-NTR, respectively. The optical purity of each enantiomer was determined to be more than 99.96%, and the amount of photo degradation product of NTR was determined to be less than 0.03% by liquid chromatography, on a CHIRALCEL OJ-H column (Daicel Chemical Industries, Ltd.,

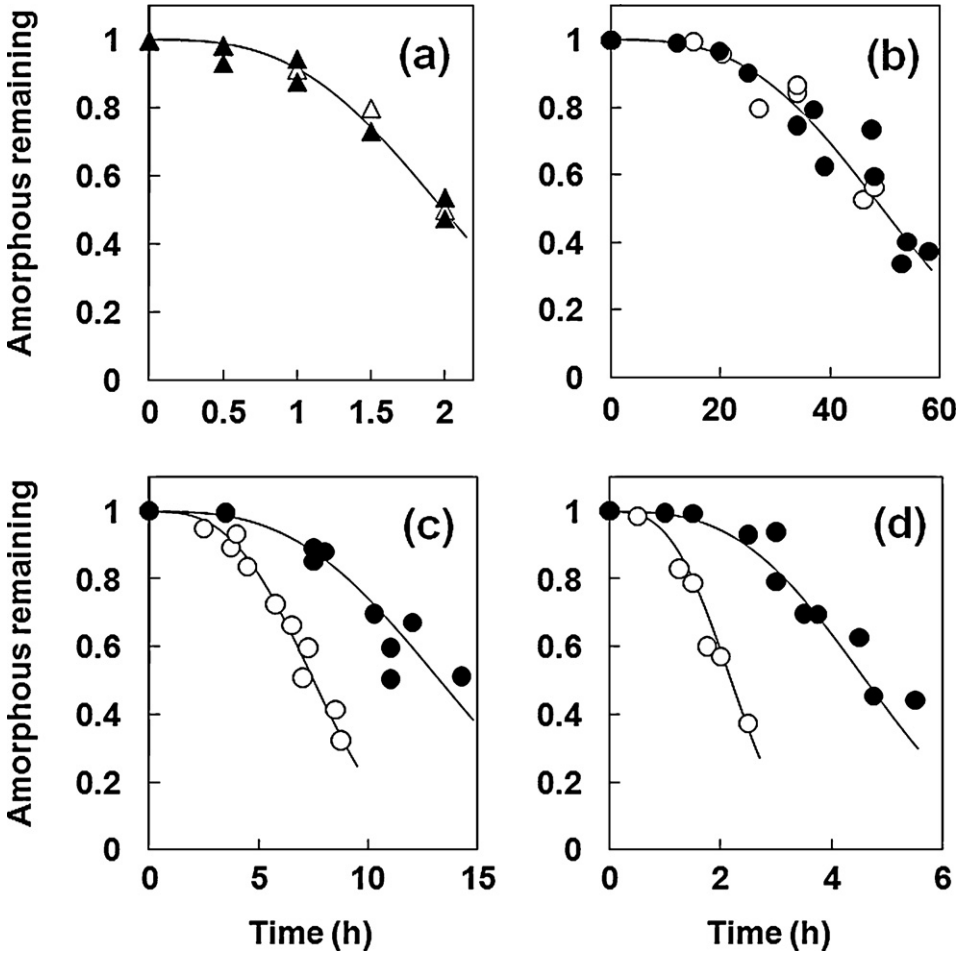

Fig. 2. Crystallization profiles of each NTR enantiomer alone ((a); △, ▲) and the enantiomers in solid dispersions (○, ●) with (b) 10% PVP, (c) 10% HPMC and (d) 10% HPMCP at 60 °C. Open symbols represent (−)-NTR and solid symbols represent (+)-NTR. The lines in the figures represent the best fit of the Avrami equation.

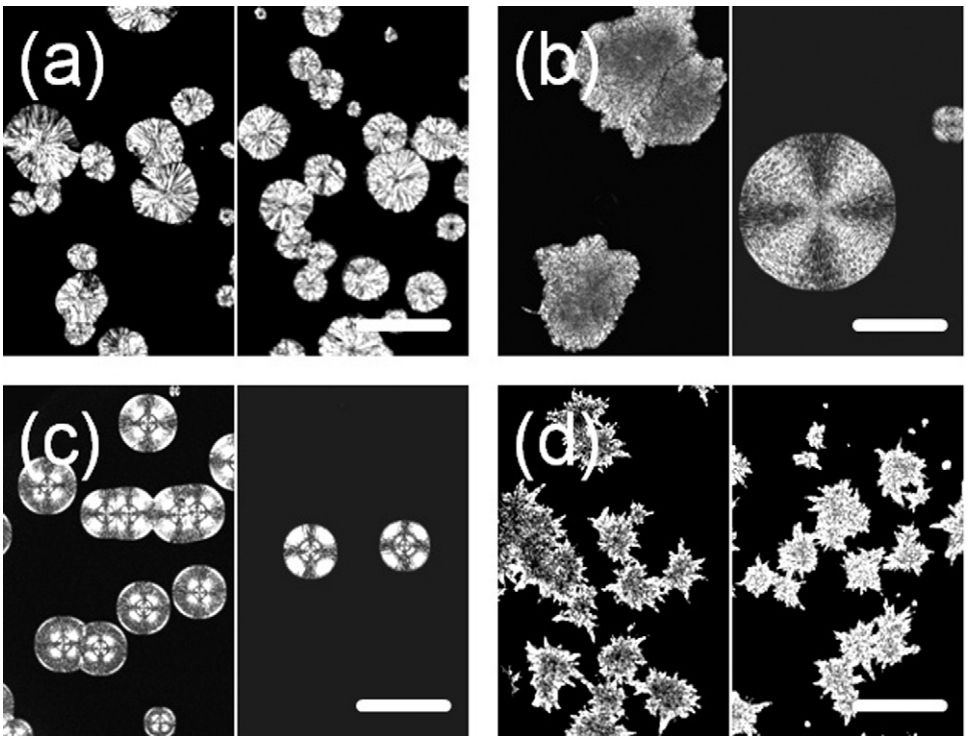

Fig. 3. Typical crystal shape observed for the amorphous NTR enantiomers and their solid dispersions: (a) without polymer, (b) 10% HPMC, (c) 10% HPMCP and (d) 10% PVP. The left side of each micrograph was taken from the (−)-NTR samples, and the right side from the (+)-NTR samples. The bars in the micrographs correspond to 100 μm.

4.6 mm × 250 mm) with a mobile phase of n-hexane/ethanol = 10/1 (1 ml/min). Since NTR is a photo sensitive compound, NTR samples were handled under dim light (<120 lx).

2.2. Determination of the overall crystallization rate of amorphous NTR enantiomers

Amorphous solid dispersions of the NTR enantiomers were prepared by melt-quenching drug–polymer mixtures. One NTR enantiomer and a polymer were initially dissolved in a solvent that was suitable for both components. Ethanol/acetone (1:1) was used for the NTR–HPMC and NTR–HPMCP combinations, and ethanol was used for the NTR–PVP combination. Next, the solvent was rotary-evaporated to obtain a homogeneous drug–polymer mixture. Approximately 4 mg of the pulverized mixture was weighed into an aluminum pan for DSC, and was kept at around 180 °C in the cell of a DSC (DSC2920, TA Instruments) for approximately 2 min under dry nitrogen gas flow (30 ml/min). The melted sample was transferred to a desiccator containing phosphorus pentoxide, and the desiccator was stored at a constant temperature of 30–70 °C. For the pure NTR enantiomer, the resolved enantiomer crystal (4 mg) was melt-quenched as described above to obtain an amorphous sample.

After certain periods of time, the change in heat capacity (ΔC_p) at T_g was measured for the stored amorphous samples by DSC at a heating rate of 20 °C/min. The amount of amorphous drug remaining in the sample at time t, $x(t)$, was calculated according to Eq. (1):

$$x(t) = \frac{\Delta C_{pt}}{\Delta C_{p0}} \quad (1)$$

where ΔC_{pt} and ΔC_{p0} are the ΔC_p values at time t and initially, respectively. The time required for 10% of the amorphous NTR to crystallize (t_{90}) was estimated as an indicator of the crystallization tendency. The time-profiles of $x(t)$ were analyzed according to the Avrami equation (Eq. (2), $n = 3$) to calculate t_{90}:

$$x(t) = \exp[-kt^n] \quad (2)$$

where k is the crystallization rate constant and n is the Avrami index. HPLC analysis of stored NTR samples showed no evidence of degradation during melt-quenching and subsequent storage.

2.3. Determination of nucleation rate and crystal growth rate of NTR enantiomer

The nucleation rate and the crystal growth rate were determined for samples prepared in a space between two glass disks separated by a stainless steel ring. The NTR enantiomer–polymer mixture, which was described above, or the crystalline NTR enantiomer (1.5–2 mg) was placed on a clean glass disk (thickness: 0.12 mm, diameter: 16 mm) and heated at 180 °C in the DSC with a stainless steel ring (inner diameter: 6 mm, thickness: 20 μm) as a spacer. After the sample had melted completely, it was covered with another glass disk (thickness: 0.12 mm, diameter: 12 mm) to yield an amorphous layer between the glasses. Attention was paid to ensure that the layer was free of bubbles. For measurements at temperatures above 40 °C, the sample was stored in the chamber of a heating/cooling stage for microscopy (THMS600, Linkam Scientific Instruments), which had been adjusted to a prescribed temperature in advance. The moisture in the chamber was removed by purging with dry nitrogen gas for 10–15 min. Microscopic images of the sample were recorded at appropriate time intervals by a digital camera (DXM1200F, Nikon Corporation) attached to a polarized light microscope (ECLIPSE E600 POL, Nikon Corporation) with a 10× objective lens. In order to minimize possible photo degradation of NTR by the polarized light, the light source of the microscope was shut off when images were not recorded. For measurements at 30 °C, the samples were stored at 30 °C in desiccators containing phosphorous pentoxide. After an appropriate period of storage, microscopic images of the sample were recorded, and the sample was again stored at 30 °C in a dry state.

2.3.1. Measurement of nucleation rate

The nucleation rate of the NTR enantiomers was estimated from time-profiles of nucleation site density determined from microscopic images of the stored samples. Nucleation site density per unit volume was calculated from the number of nucleation sites per unit area and the depth of field of the lens used for data collection. The depth of field was calculated to be 8.46 μm from the wavelength of the light (546 nm) and the numerical aperture of the lens (0.25). For samples with more than a dozen nucleation sites per fixed field at the end of the observation period, nucleation sites were counted in one fixed field. For samples with less than a dozen nucleation sites per field near the end of the observation period, and those stored at 30 °C, nucleation sites were counted for 12 individual areas in one sample, and the average value from the 12 individual images was regarded as the number of nucleation sites per field. The nucleation rate was obtained from the slope of time-profiles of the number of nucleation sites per unit volume (nucleation site density) at steady state. In cases showing preferential nucleation and growth at the sample periphery, these sites were not included in the analysis. The reported nucleation rates were average values of those obtained for at least three samples prepared separately.

2.3.2. Measurement of crystal growth rate

The crystal growth rates at temperatures above 40 °C were measured concurrently with the nucleation rate measurements as described above. The measurements at 30 °C were carried out using samples that showed more than a dozen nucleation sites per one field after a few months of storage in desiccators containing phosphorous pentoxide. The sample was placed in the chamber of the heating/cooling stage controlled at 30 °C, and the growth of crystals was observed in a fixed field. The radius of each crystal was estimated from a circular approximation by using Lumina Vision software (Mitani Co.). The average crystal growth rate was calculated from the increase in the radius as a function of time based on observations of at least 20 crystals.

2.4. FT-IR

FI-IR spectra were collected using a FT/IR-6300 (JASCO Corporation) by the KBr method at ambient room temperature. Transmission spectra were obtained for KBr disks containing 1–1.5% sample at a resolution of 0.4 cm^{-1} within the range of 4000–400 cm^{-1}. An accumulation of 128–256 scans was acquired for each disk.

3. Results

3.1. Effects of polymers on the overall crystallization rates of NTR enantiomers in solid dispersions

No significant differences in the melting point (158 °C), T_g (33 °C) and ΔC_p at T_g (0.40 J/g/K) were observed between (−)-NTR and (+)-NTR. Table 1 shows the T_g values of amorphous solid dispersions of (−)-NTR and (+)-NTR. There appeared to be no significant difference in the T_g values between the two. The solid dispersions containing HPMC (10–20%) and 5% PVP showed T_g values similar to that of each NTR enantiomer alone. T_g values for solid dispersions containing 10% PVP were slightly higher than that of each NTR enantiomer alone, whereas solid dispersions containing HPMCP (10–20%) exhibited T_g values slightly lower than that of each NTR enantiomer alone.

Fig. 2 shows time-profiles of overall crystallization of NTR enantiomers at 60 °C. No significant differences in the overall crystallization profiles were observed between (−)-NTR and (+)-NTR without polymer (Fig. 2(a)), and between (−)-NTR and (+)-NTR in solid dispersions containing 10% PVP (Fig. 2(b)). In contrast, differences in time-profiles between the enantiomers were observed for solid dispersions containing 10% HPMC or HPMCP: (+)-NTR crystallized more slowly than (−)-NTR, as shown in Fig. 2(c) and (d). Table 2 shows the t_{90} values for the amorphous NTR enantiomers obtained for NTR alone and NTR in the solid dispersions. The t_{90} values for (−)-NTR without polymer and those of solid dispersions containing 5–10% PVP were almost the same as the t_{90} values for (+)-NTR without polymer and those of solid dispersions containing 5–10% PVP, respectively, at the temperatures studied. The t_{90} values at 50 and 60 °C for (+)-NTR were 1.5–2.0 times longer than that for (−)-NTR in solid dispersions containing 10–20% HPMC or HPMCP. At 40 °C, however, any difference between the enantiomers was not clear.

Table 1
T_g of pure NTR enantiomers and their solid dispersions with a polymer.

Polymer	Polymer content [%]	T_g[a] [°C]	
		(−)-NTR	(+)-NTR
None	0	33.2 ± 0.1	33.1 ± 0.2
HPMC	10	33.1 ± 1.0	33.0 ± 0.7
	20	33.1 ± 0.8	33.0 ± 0.7
HPMCP	10	31.2 ± 0.7	31.0 ± 0.4
	20	30.8 ± 1.2	30.5 ± 0.9
PVP	5	33.0 ± 0.2	33.1 ± 0.2
	10	36.3 ± 1.2	36.2 ± 0.8

[a] Average ± standard deviation (n = 3).

3.2. Effects of polymers on the nucleation rate and crystal growth rate

Fig. 3 shows the typical micrographs of NTR crystals grown from amorphous pure enantiomers and their solid dispersions with a polymer. The recrystallized NTR enantiomers without polymers showed a melting point of 158 °C, suggesting the same crystal form as the originally resolved stable one. The melting point of the samples containing 10% HPMC, HPMCP and PVP was approximately 151 °C in all cases, regardless of the various crystal shapes shown in Fig. 3. The difference from the melting point of the pure enantiomers would have been due to melting point depression by the

Table 2
t_{90} for NTR enantiomers with and without polymer.

Temperature [°C]	Polymer	[%]	t_{90}[a] [h]			
			(−)-NTR		(+)-NTR	
40	None	0	41	(1)	41	(1)
	HPMC	10	230, 240[b]		230, 230[b]	
	HPMCP	10	49	(1)	49	(1)
50	None	0	5.7	(0.2)	5.7	(0.1)
	PVP	10	250	(10)	240	(4)
	HPMC	10	17	(0.4)	25	(0.1)
	HPMCP	10	6.1	(0.3)	11	(0.3)
60	None	0	1.1	(0.1)	1.1	(0.1)
	PVP	5	3.5	(0.1)	3.6	(0.1)
		10	25 ± 3[c]		25 ± 3[c]	
	HPMC	10	3.8, 4.1[b]		6.7, 6.9[b]	
		20	8.7	(0.3)	15	(0.4)
	HPMCP	10	1.5 ± 0.2[c]		2.7 ± 0.3[c]	
		20	3.2	(0.1)	6.4	(0.2)

[a] The values in parentheses are standard error estimated from single experiments using Origin 8.1 software (Lightstone Corp.).
[b] Results with two values represent the results obtained from duplicate experiments using separately prepared samples.
[c] Mean ± standard deviation (n = 3).

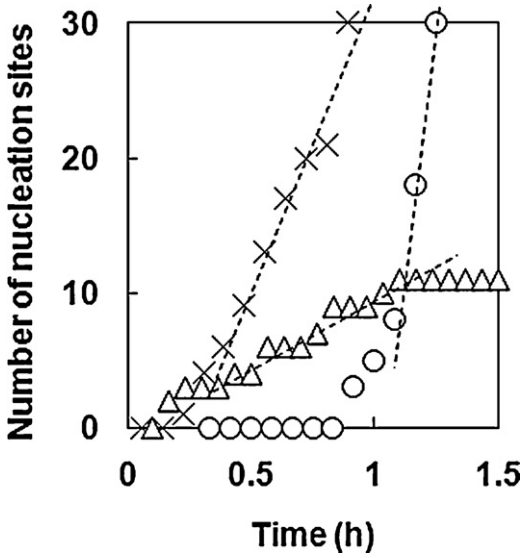

Fig. 4. Time profiles of the number of nucleation sites per field of view for (+)-NTR at 50 °C (○), 60 °C (×) and 70 °C (△). The dotted lines show the linear regression at steady state.

added polymers, as the melting point fell gradually with increasing polymer content (data not shown). The data suggested that differences in crystal habit, rather than polymorphism, might have been responsible for the differences in crystal shape among the solid dispersions.

Fig. 4 shows the typical time-profiles of the nucleation of amorphous NTR enantiomer stored at various temperatures. The lower the storage temperature, the longer the period required before the first crystal was observed. The nucleation rates at steady state were obtained from the slope of the lines in Fig. 4, and these were plotted against storage temperature (Fig. 5). As expected from the similar overall crystallization profiles of the NTR enantiomers (Fig. 2(a) and (b)), no significant difference in the nucleation rates between (−)-NTR and (+)-NTR was observed for amorphous NTR alone and the solid dispersions containing PVP within the temperature range studied (Fig. 5(a)). In contrast, the nucleation rates of (+)-NTR were lower than those of (−)-NTR in the solid dispersions containing HPMC and HPMCP (Fig. 5(b)) within the temperature range of 50–70 °C. At 40 °C, however, the differences in the rates between (−)-NTR and (+)-NTR were not pronounced. These results were consistent with the t_{90} values of the enantiomers shown in Table 2.

Fig. 6 shows the typical time-profiles of the NTR crystal growth at 60 °C. Crystal radius increased linearly with time, and the growth rate was estimated from linear regression of the plots. The higher the temperature, the faster the crystals grew within the temperature range studied (Fig. 7). In contrast to the nucleation rates, no significant growth rate differences between the NTR enantiomers were observed, irrespective of the absence or presence of any polymer.

3.3. FT-IR

FT-IR spectra (4000–400 cm^{-1}) of (−)-NTR and (+)-NTR were indistinguishable from one another for both the amorphous and the crystalline forms. Similarly, the FT-IR spectra of amorphous solid dispersions were almost the same for (−)-NTR and (+)-NTR with any polymer. Fig. 8 shows the spectra for crystalline (−)-NTR (dotted line in Fig. 8 (a)), NTR solid dispersions containing 25–75% HPMC and HPMC alone (dotted line in Fig. 8 (c)) in the range of 1800–1550 cm^{-1}, corresponding to C=O stretching region of NTR. Spectra with and without an asterisk represent that of (−)-NTR

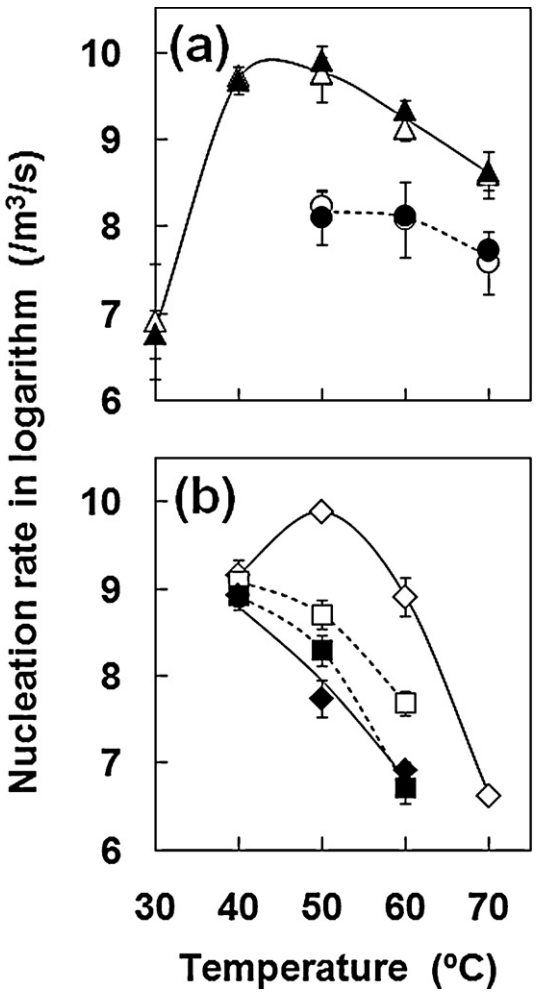

Fig. 5. Plots of nucleation rate as a function of temperature. Error bars represent standard deviation for at least triplicate experiments. (a) △, ▲: without polymer, ○, ●: 10% PVP and (b) □, ■: 10% HPMC, ◇, ♦: 10% HPMCP. Open symbols represent (−)-NTR and solid symbols represent (+)-NTR.

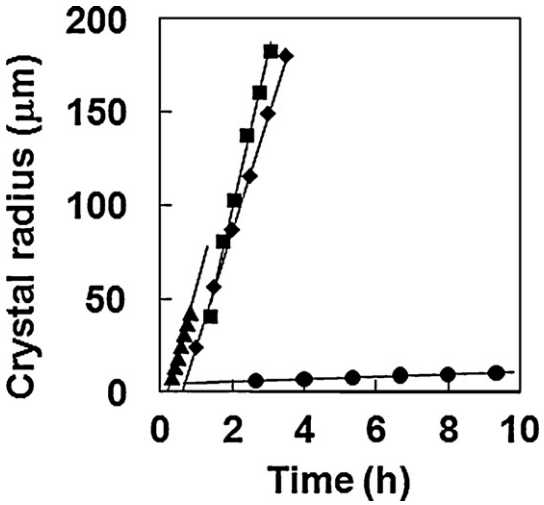

Fig. 6. Typical time profiles of the radius of NTR crystals in (+)-NTR alone (▲), and solid dispersions with 10% HPMC (■), 10% HPMCP (♦) and 10% PVP (●) at 60 °C.

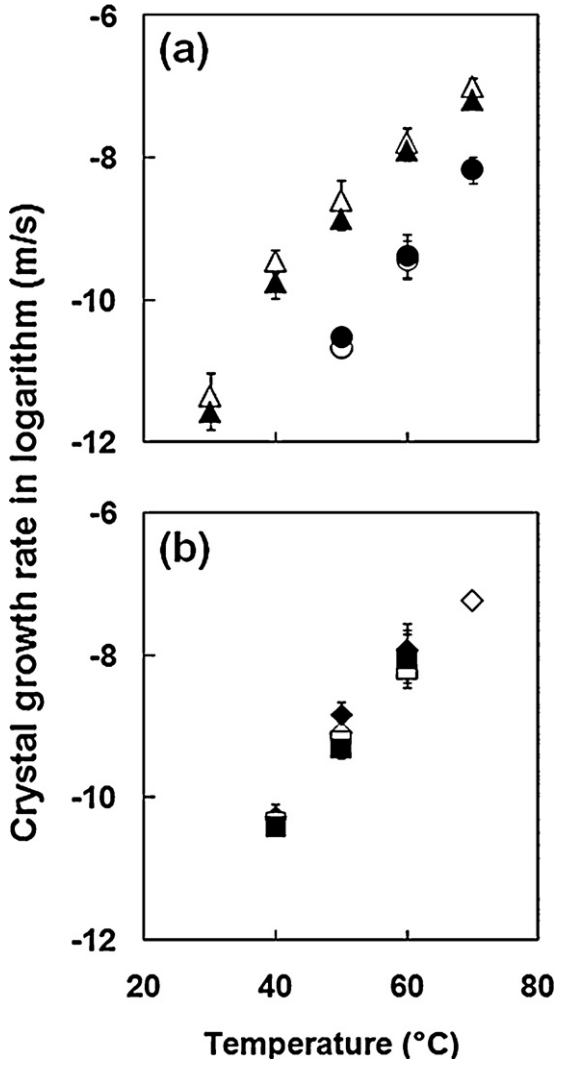

Fig. 7. Temperature dependence of crystal growth rate of NTR enantiomers. Error bars represent standard deviation for at least triplicate experiments. (a) △, ▲: without polymer; ○, ●: 10% PVP and (b) □, ■: 10% HPMC; ◇, ◆: 10% HPMCP. Open symbols represent (−)-NTR and solid symbols represent (+)-NTR.

and (+)-NTR, respectively. Despite its vicinity to the asymmetric carbon, carbonyl group of (−)-NTR and (+)-NTR showed same spectra even in the presence of HPMC. Likewise, no difference in spectra between solid dispersions of (−)-NTR and (+)-NTR containing HPMCP was observed (data not shown).

Fig. 9 shows the spectra in the range of 3650–3150 cm^{-1}, corresponding to NH stretching vibrations of nifedipine derivatives (Konno and Taylor, 2006), where the changes in peak position were obvious upon mixing with polymers as solid dispersions. There were also no obvious differences in the spectra between the two enantiomers. The peak around 3350 cm^{-1} was assigned to the NH stretching vibration that was expected to be involved in the hydrogen bonding between the drug and a polymer. The peak position was shifted from 3360 cm^{-1} to 3337 cm^{-1} by amorphization, and additionally shifted to 3291 cm^{-1} in the presence of 50% PVP (Figs. 9(b) and 10). On the other hand, for solid dispersions prepared with HPMC and HPMCP, the peak position showed a degree of shift to a higher wavenumber (Figs. 9(c) and (d) and 10). The peak position for solid dispersions with 75% HPMCP was nearly equal to that of the pure NTR crystals. These changes in peak position showed the same tendency for both (+)-NTR and (−)-NTR.

4. Discussion

The overall crystallization of (−)-NTR proceeded faster than that of (+)-NTR in solid dispersions with HPMC or HPMCP (Fig. 2(c) and (d)), while that for solid dispersions with PVP proceeded at almost the same rate, regardless of NTR chirality (Fig. 2(b)). The nucleation rates of (−)-NTR were greater than those of (+)-NTR in solid dispersions with HPMC or HPMCP at 50–70 °C (Fig. 5(b)), while no difference in nucleation rates between the NTR enantiomers was observed for solid dispersions with PVP (Fig. 5(a)). The T_g values for samples using (−)-NTR or (+)-NTR were almost the same (Table 1), suggesting that the differences in the overall crystallization profiles and nucleation rates between the enantiomers are not due to differences in molecular mobility between (−)-NTR and (+)-NTR in solid dispersions with HPMC or HPMCP. The difference in physical stability between the two enantiomers may be explained by the difference in strength of NTR–polymer interaction between them. The results obtained from FT-IR measurements indicate that PVP interacts with NTR through hydrogen bonding at the NH moiety of NTR (Figs. 9 and 10). Almost the same degrees of shift in wavenumber for NH stretching suggest a similar strength of hydrogen bond interaction for (−)-NTR and (+)-NTR. PVP polymer chains possess an asymmetric carbon in a monomer unit, and are composed of monomer units with an equal ratio of R and S configurations. Therefore, (−)-NTR and (+)-NTR are considered to interact with PVP through hydrogen bonds of the same strength and number, resulting in a similar degree of physical stability between (−)-NTR and (+)-NTR. In contrast, HPMC and HPMCP are cellulose derivatives that are polymers of optically active D-glucose, and thus are expected to interact differently (strength and/or number) with NTR enantiomers, resulting in the difference in physical stability between (−)-NTR and (+)-NTR, although differences in interaction were not detectable by FT-IR. At 40 °C, however, the differences in physical stability between the enantiomers with HPMC or HPMCP were not remarkable (Table 2, Fig. 5). We do not have a satisfactory explanation for the loss of the difference in stabilization by HPMC and HPMCP. However, one possible explanation is as follows: The temperature dependence of the nucleation rate exhibits a maximum just above T_g because the nucleation rate is influenced by both molecular mobility and thermodynamic factors; an increase of temperature increases the molecular mobility, and thus the nucleation rate, whereas nucleation is thermodynamically favored at lower temperatures. A barrier due to molecular mobility is considered to play a predominant role in nucleation within the temperature range below the maximum point (Hancock and Zografi, 1997; Andronis and Zografi, 2000). Therefore, loss of the difference in physical stability between the enantiomers at 40 °C may be due to the predominant contribution of molecular mobility, since the molecular mobility is suggested to be similar for (−)-NTR and (+)-NTR in solid dispersions, as indicated by the T_g values (Table 1). However, physical stability data at temperatures below 40 °C, which are difficult to obtain within the commonly used experimental time scale, are needed in order to support this speculation.

In contrast to the nucleation rates, no significant difference in the crystal growth rates between the NTR enantiomers was observed for solid dispersions with HPMC or HPMCP (Fig. 7). The crystal growth rates for solid dispersions with HPMC or HPMCP were similar to those for each NTR enantiomer alone, indicating that the effects of HPMC and HPMCP on the crystal growth rate were small. This might be one of the reasons why differences in the crystal growth rate between the NTR enantiomers could not be detected in solid dispersions with HPMC or HPMCP.

It may be worth to note that PVP decreased the crystal growth rate of NTR enantiomers more than HPMC and HPMCP at all the temperatures studied (Fig. 7). On the other hand, PVP did not always decrease the nucleation rate of NTR more effectively than HPMC or

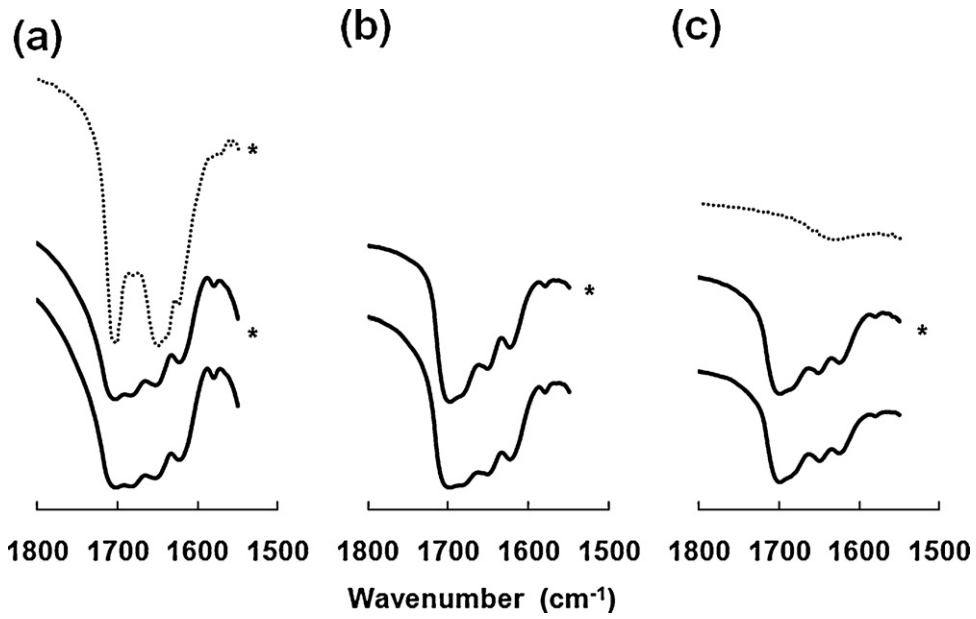

Fig. 8. FT-IR spectra of crystalline (−)-NTR, solid dispersions of NTR enantiomer containing HPMC, and HPMC alone. HPMC content was (a) 25% (b) 50%, and (c)75%. Dotted line in (a) represents the spectrum for crystalline (−)-NTR, and dotted line in (c) represents the spectrum for HPMC alone. The spectra with an asterisk are those of (−)-NTR.

HPMCP. For example, the nucleation rate of NTR at 60°C was following order; (−)-NTR, (+)-NTR ≈ (−)-NTR–HPMCP > (−)-NTR–PVP, (+)-NTR–PVP > (−)-NTR–HPMC > (+)-NTR–HPMC, (+)-NTR–HPMCP (Fig. 5). PVP seems to decrease the crystal growth rate more effectively than the nucleation rate of NTR, whereas HPMC and HPMCP decrease only the nucleation rate of NTR. The reason for the different stabilizing effects of the polymers for the nucleation and crystal growth of NTR is not clear. The growth rate of NTR may only be decreased by strong interactions such as hydrogen bonding between NTR and PVP, which is detectable by FT-IR (Figs. 9 and 10). Weak drug–polymer interactions, which are not detectable by FT-IR, may decrease the nucleation rate of NTR, as well as hydrogen bond interactions between drug and polymer.

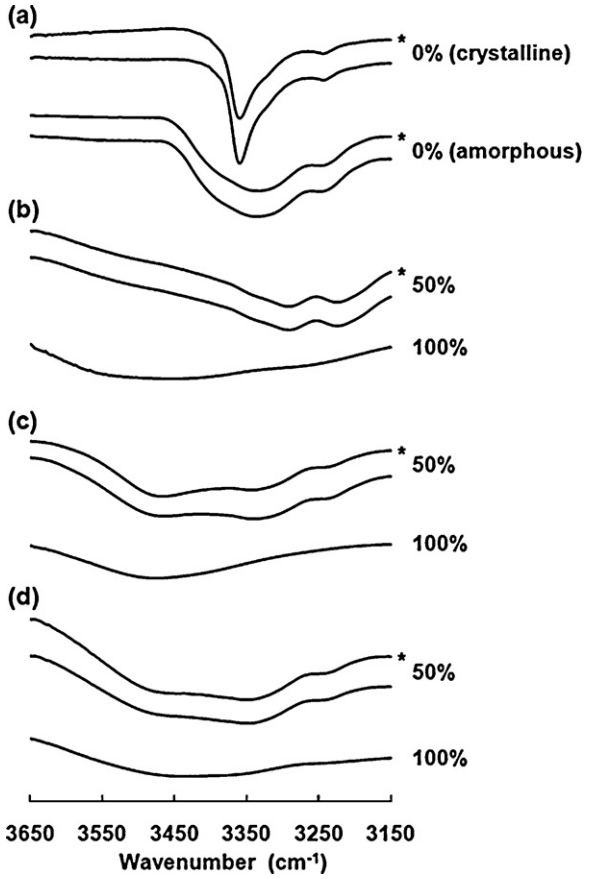

Fig. 9. FT-IR spectra of (a) crystalline and amorphous NTR enantiomers, and their amorphous solid dispersions with (b) PVP, (c) HPMC and (d) HPMCP. Percentages represent the weight percentage of polymer in the solid dispersions. The spectra with an asterisk are those of (−)-NTR.

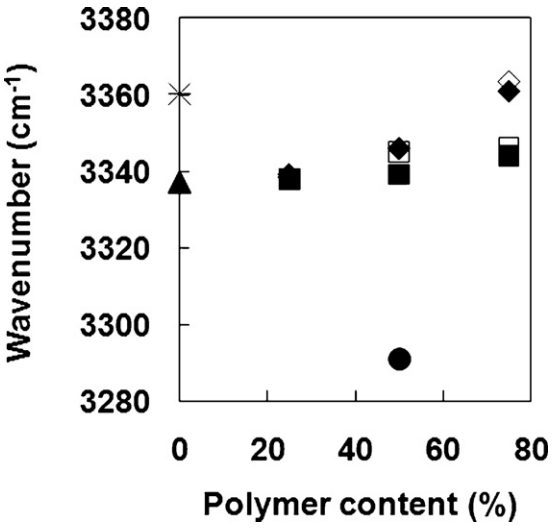

Fig. 10. Changes in FT-IR peak position showing the NH stretching region. +: (−)-NTR without polymer (crystalline); ×: (+)-NTR without polymer (crystalline); △, ▲: without polymer (amorphous); □, ■: HPMC; ♢, ♦: HPMCP; ○, ●: PVP. Open symbols represent (−)-NTR and solid symbols represent (+)-NTR.

5. Conclusions

Using NTR enantiomers as model drugs, the effects of stereoselective drug–polymer interaction on the crystallization rate of amorphous solid dispersions were elucidated. The chiral polymers, HPMC and HPMCP, retarded the crystallization of (+)-NTR more

effectively than that of (−)-NTR. The difference in physical stability at 50–70 °C would be due to stereoselective interaction. Stereoselective interaction affected the nucleation process more markedly than the crystal growth process. Since the stereoselective interaction between NTR enantiomers and HPMC or HPMCP would have been relatively weak, the impact of the interaction on the physical stability of amorphous NTR solid dispersions was obscure at room temperature.

Acknowledgements

Part of this work was supported by a Grant-in-aid for Research on Publicly Essential Drugs and Medical Devices from the Japan Health Sciences foundation.

References

Andronis, V., Zografi, G., 2000. Crystal nucleation and growth of indomethacin polymorphs from the amorphous state. J. Non-Cryst. Solids 271, 236–248.

Aso, Y., Yoshioka, S., Kojima, S., 2004. Molecular mobility-based estimation of the crystallization rates of amorphous nifedipine and phenobarbital in poly(vinylpyrrolidone) solid dispersions. J. Pharm. Sci. 93, 384–391.

Chutimaworapan, S., Ritthidej, G.C., Yonemochi, E., Oguchi, T., Yamamoto, K., 2000. Effect of water-soluble carriers on dissolution characteristics of nifedipine solid dispersions. Drug Dev. Ind. Pharm. 26, 1141–1150.

Haddadin, R., Qian, F., Desikan, S., Hussain, M., Smith, R.L., 2009. Estimation of drug solubility in polymers via differential scanning calorimetry and utilization of the fox equation. Pharm. Dev. Technol. 14, 18–26.

Hancock, B.C., Zografi, G., 1997. Characteristics and significance of the amorphous state in pharmaceutical systems. J. Pharm. Sci. 86, 1–12.

Hirasawa, N., Ishise, S., Miyata, H., Danjo, K., 2003a. Physicochemical characterization and drug release studies of nilvadipine solid dispersions using water-insoluble polymer as a carrier. Drug Dev. Ind. Pharm. 29, 339–344.

Hirasawa, N., Ishise, S., Miyata, H., Danjo, K., 2003b. An attempt to stabilize nilvadipine solid dispersion by the use of ternary systems. Drug Dev. Ind. Pharm. 29, 997–1004.

Hirasawa, N., Ishise, S., Miyata, H., Danjo, K., 2004. Application of nilvadipine solid dispersion to tablet formulation and manufacturing using crospovidone and methylcellulose as dispersion carriers. Chem. Pharm. Bull. 52, 244–247.

Huang, J., Wigent, R.J., Schwartz, J.B., 2008. Drug–polymer interaction and its significance on the physical stability of nifedipine amorphous dispersion in microparticles of an ammonio methacrylate copolymer and ethylcellulose binary blend. J. Pharm. Sci. 97, 251–262.

Karavas, E., Ktistis, G., Xenakis, A., Georgarakis, E., 2005. Miscibility behavior and formation mechanism of stabilized felodipine-polyvinylpyrrolidone amorphous solid dispersions. Drug Dev. Ind. Pharm. 31, 473–489.

Karavas, E., Ktistis, G., Xenakis, A., Georgarakis, E., 2006. Effect of hydrogen bonding interactions on the release mechanism of felodipine from nanodispersions with polyvinylpyrrolidone. Eur. J. Pharm. Biopharm. 63, 103–114.

Kim, E.J., Chun, M.K., Jang, J.S., Lee, I.H., Lee, K.R., Choi, H.K., 2006. Preparation of a solid dispersion of felodipine using a solvent wetting method. Eur. J. Pharm. Biopharm. 64, 200–205.

Konno, H., Taylor, L.S., 2006. Influence of different polymers on the crystallization tendency of molecularly dispersed amorphous felodipine. J. Pharm. Sci. 95, 2692–2705.

Marsac, P.J., Shamblin, S.L., Taylor, L.S., 2006. Theoretical and practical approaches for prediction of drug–polymer miscibility and solubility. Pharm. Res. 23, 2417–2426.

Marsac, P.J., Konno, H., Rumondor, A.C., Taylor, L.S., 2008. Recrystallization of nifedipine and felodipine from amorphous molecular level solid dispersions containing poly(vinylpyrrolidone) and sorbed water. Pharm. Res. 25, 647–656.

Marsac, P.J., Li, T., Taylor, L.S., 2009. Estimation of drug–polymer miscibility and solubility in amorphous solid dispersions using experimentally determined interaction parameters. Pharm. Res. 26, 139–151.

Marsac, P.J., Rumondor, A.C., Nivens, D.E., Kestur, U.S., Stanciu, L., Taylor, L.S., 2010. Effect of temperature and moisture on the miscibility of amorphous dispersions of felodipine and poly(vinyl pyrrolidone). J. Pharm. Sci. 99, 169–185.

Matsumoto, T., Zografi, G., 1999. Physical properties of solid molecular dispersions of indomethacin with poly(vinylpyrrolidone) and poly(vinylpyrrolidone-co-vinylacetate) in relation to indomethacin crystallization. Pharm. Res. 16, 1722–1728.

Miyazaki, T., Yoshioka, S., Aso, Y., Kojima, S., 2004. Ability of polyvinylpyrrolidone and polyacrylic acid to inhibit the crystallization of amorphous acetaminophen. J. Pharm. Sci. 93, 2710–2717.

Miyazaki, T., Yoshioka, S., Aso, Y., 2006. Physical stability of amorphous acetanilide derivatives improved by polymer excipients. Chem. Pharm. Bull. 54, 1207–1210.

Miyazaki, T., Yoshioka, S., Aso, Y., Kawanishi, T., 2007. Crystallization rate of amorphous nifedipine analogues unrelated to the glass transition temperature. Int. J. Pharm. 336, 191–195.

Rumondor, A.C., Marsac, P.J., Stanford, L.A., Taylor, L.S., 2009a. Phase behavior of poly(vinylpyrrolidone) containing amorphous solid dispersions in the presence of moisture. Mol. Pharm. 6, 1492–1505.

Rumondor, A.C.F., Ivanisevic, I., Bates, S., Alonzo, D.E., Taylor, L.S., 2009b. Evaluation of drug–polymer miscibility in amorphous solid dispersion systems. Pharm. Res. 26, 2523–2534.

Suzuki, H., Sunada, H., 1998. Influence of water-soluble polymers on the dissolution of nifedipine solid dispersions with combined carriers. Chem. Pharm. Bull. 46, 482–487.

Tanno, F., Nishiyama, Y., Kokubo, H., Obara, S., 2004. Evaluation of hypromellose acetate succinate (HPMCAS) as a carrier in solid dispersions. Drug Dev. Ind. Pharm. 30, 9–17.

Tao, J., Sun, Y., Zhang, G.G., Yu, L., 2009. Solubility of small-molecule crystals in polymers: D-mannitol in PVP, indomethacin in PVP/VA, and nifedipine in PVP/VA. Pharm. Res. 26, 855–864.

Telang, C., Mujumdar, S., Mathew, M., 2009. Improved physical stability of amorphous state through acid base interactions. J. Pharm. Sci. 98, 2149–2159.

Vippagunta, S.R., Maul, K.A., Tallavajhala, S., Grant, D.J.W., 2002. Solid-state characterization of nifedipine solid dispersions. Int. J. Pharm. 236, 111–123.

Wang, L., Cui, F.D., Hayase, T., Sunada, H., 2005. Preparation and evaluation of solid dispersion for nitrendipine–carbopol and nitrendipine–HPMCP systems using a twin screw extruder. Chem. Pharm. Bull. 53, 1240–1245.

Wang, L., Cui, F.D., Sunada, H., 2007. Improvement of the dissolution rate of nitrendipine using a new pulse combustion drying method. Chem. Pharm. Bull. 55, 1119–1125.